Lensless Diffractive Imaging Using Tabletop Coherent High-Harmonic Soft-X-Ray Beams

Richard L. Sandberg,* Ariel Paul, Daisy A. Raymondson, Steffen Hädrich, David M. Gaudiosi, Jim Holtsnider, Ra'anan I. Tobey, Oren Cohen, Margaret M. Murnane, and Henry C. Kapteyn

JILA and Department of Physics, University of Colorado and NSF Engineering Research Center in Extreme Ultraviolet Science and Technology, Boulder, Colorado 80309, USA

Changyong Song and Jianwei Miao

Department of Physics and Astronomy, University of California, Los Angeles, California 90095, USA

Yanwei Liu and Farhad Salmassi

Center for X-Ray Optics, Lawrence Berkeley National Laboratory, Berkeley, California 94720, USA

(Received 18 April 2007; published 29 August 2007)

We present the first experimental demonstration of lensless diffractive imaging using coherent soft x rays generated by a tabletop soft-x-ray source. A 29 nm high harmonic beam illuminates an object, and the subsequent diffraction is collected on an x-ray CCD camera. High dynamic range diffraction patterns are obtained by taking multiple exposures while blocking small-angle diffraction using beam blocks of varying size. These patterns reconstruct to images with 214 nm resolution. This work demonstrates a practical tabletop lensless microscope that promises to find applications in materials science, nanoscience, and biology.

DOI: 10.1103/PhysRevLett.99.098103 PACS numbers: 87.59.−e, 61.10.−i, 41.50.+h, 42.65.−k

Microscopy has been a critical enabling technology for understanding materials and biological systems since its invention. Using innovative imaging and labeling techniques, visible light microscopes can image living cells with a resolution as high as 200 nm [1]. However, this resolution is fundamentally limited by the wavelength of light in the visible to near-UV range. To further increase resolution, the much shorter wavelength of moderate-energy electrons can be used, and atomic level resolution has been demonstrated in electron microscopy [2]. However, electron microscopes are limited by the mean-free-path of the charged particles, and therefore this technique is restricted to imaging thin samples, typically $<$500 nm. Many biological specimens, as well as samples of interest for materials science, are too thick for electron microscopy. Furthermore, low contrast in electron microscopy also requires sophisticated labeling techniques. Thus, new techniques for nanomicroscopy are of great interest.

One of the most promising alternative approaches for high-resolution imaging of thicker samples is to use shorter wavelength light, in the extreme ultraviolet (EUV) or soft-x-ray (SXR) regions of the spectrum [3]. EUV or SXR light can be used for nondestructive imaging applications requiring high resolution in thick samples [4]. Furthermore, numerous core-level absorption edges and widely varying elemental absorption cross sections provide excellent inherent image contrast, particularly for biological imaging in the "water window" (300 eV–500 eV) region of the spectrum, or for magnetic domain imaging around 800 eV [3–6]. Successful soft-x-ray imaging techniques use diffractive or reflective optics such as Fresnel zone plates or multilayer mirrors, since the very strong absorption by matter and low index contrast of materials at short wavelengths precludes the use of refractive optics. Zone-plate imaging has been demonstrated at resolutions as high as 15 nm using state-of-the-art diffractive optics at synchrotron sources [7], while zone-plate imaging with tabletop high harmonic sources can achieve resolutions of $\approx$ 200 nm [8]. Zone plates require very careful manufacturing, with feature sizes equal to the desired resolution, and dimensional tolerances several times smaller. Furthermore, microscopes based on zone-plate optics have a relatively short depth of field.

Lensless imaging is a relatively new coherent imaging technique that is complementary to zone-plate imaging [9–13]. This technique requires spatially coherent beams and eliminates imaging elements in the optical system by replacing them with a computerized phase retrieval algorithm. By obviating the need for an imaging system, lensless imaging is well-suited to x rays, and it was first demonstrated in 1999 using spatially filtered light from a synchrotron source [9]. In lensless imaging, the x-ray beam illuminates an object, and the scatter pattern (diffracted light) from the object is collected on an x-ray CCD camera. For this technique to work, the diffraction pattern must be oversampled, i.e., the diffraction peaks coming from the highest spatial frequency of interest must be sampled at a higher rate than the Nyquist criterion [14]. If a sharp diffraction pattern has been obtained and the oversampling requirement is met, the image can be reconstructed using iterative algorithms that retrieve both its amplitude and phase [15].

Given the need for *coherent* illumination, most small-scale EUV/SXR sources are not suitable for lensless imag-

ing. Thus, to date, lensless imaging has been the sole domain of large x-ray facilities such as synchrotrons or free-electron lasers, where the bright beams can be made coherent by spatial filtering. Recently, the first lensless imaging using a soft-x-ray free-electron laser facility at 32 nm was demonstrated. In that work, the high per-pulse energy of the FEL allowed single shot diffraction data to be collected [16]. However, because the sample was destroyed in the process, multiple exposures to increase the dynamic range of the data were not possible, and low spatial frequency information about the sample was missing.

High harmonic generation in gas-filled waveguide generates spatially coherent EUV beams and is ideally suited for lensless imaging [17,18]. This light source has already been used for Gabor holography with resolution <10 μm [17]. Although Gabor holography and lensless imaging are both coherent imaging techniques, geometric and flux considerations make lensless imaging better suited to high resolution imaging in a compact geometry. Here, we present the first experimental demonstration of lensless imaging using a tabletop source of coherent soft x rays. By taking multiple exposures while blocking small-angle scattered light using beam blocks of varying size, we obtain very high dynamic range diffraction patterns which successfully reconstruct to images with resolution near 200 nm. Moreover, no low spatial frequency information is missing from the reconstructions. This work thus demonstrates that lensless diffractive imaging can be successfully implemented using tabletop light sources, with broad potential application in nanoimaging and biological imaging.

The setup is shown in Fig. 1. In our experiment, 1.3 mJ, 25 fs pulses from a Ti:sapphire laser amplifier system (KMLabs Dragon^{TM}) are focused into a gas-filled waveguide at intensities of 5×10^{14} W cm^{-2}. Phase matching of the conversion process is achieved by pressure tuning the gas. In this regime, bright emission over a comb of odd-order harmonics from 25–31 is obtained at wavelengths near 30 nm [19,20]. The hollow waveguide is a 150 μm inner diameter, 10 cm long fused silica capillary filled with argon gas at $\sim$65 Torr pressure. When optimally coupled, an EUV beam is generated with a radius of 25 μm, a divergence of 1 mrad, and a flux of $\sim 10^{12}$ photons/s. Two 200 nm thick aluminum filters are used to eliminate the fundamental laser light (one is held in a custom light-tight fixture). A pair of narrowband, Mo/Si multilayer mirrors centered at $\sim$29 nm acts as both a monochromator and a condenser to gently focus the beam onto the sample with a beam waist of a few hundred microns. The narrowband mirrors each have a reflectivity of 25% in a 2.5 nm bandpass, to effectively select a single harmonic order. The sample is held in an x-y stage controlled by high-precision closed-loop dc motors. The diffraction of the EUV light from the sample is recorded on a large-area x-ray CCD camera (Andor) with a 2048×2048 array of 13.5 μm pixels.

Beam blocks of varying size are placed in the center of the diffraction pattern to block the intense diffraction coming from low spatial frequencies. A large-diameter beam block (> 1 mm) allows us to acquire long exposure images to record the highest spatial frequencies diffracted from the sample, while a small beam block (< 200 μm diameter) is used to record low spatial frequencies. These diffraction patterns are then stitched together, essentially extending the dynamic range of the camera from 4 to 12 orders of magnitude. These beam blocks are supported by a 12.5 μm wire tethered to a 2-inch diameter mounting ring, held in a kinematic x-y lens translator which allows fine control of the beam block position.

A high quality, uniform soft-x-ray mode is needed for lensless imaging to ensure the highest spatial coherence and sharpest diffraction data. Figure 1 shows the mode profile of the 29 nm EUV beam, which fits to a near-perfect Gaussian to the full dynamic range of the camera ($\approx 10^4$). The sample is carefully placed to optimize the illumination, diffraction quality, and oversampling ratio. A flat EUV intensity profile, with a variation less than 10%, is required. Overfilling the sample leads to a flatter intensity and also tends to ensure long-term illumination stability, mode quality, and a large radius of curvature of the soft-x-ray beam compared to the aperture size. The sample also must be placed far enough from the detector to guarantee a far field diffraction pattern, given by $z > \frac{D^2}{\lambda}$, where z is the sample to CCD distance, D is the sample diameter, and λ is the wavelength. Finally, the distance from the sample to the CCD is chosen to give an appropriate linear oversampling ratio (> 5) that allows for easily reconstructible diffraction patterns with high resolution [21]. The linear over-

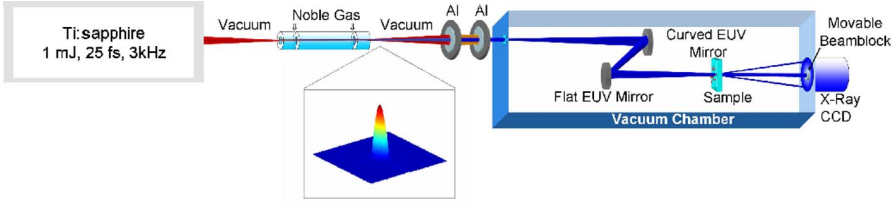

FIG. 1 (color online). Experimental setup for lensless imaging using coherent high harmonic beams at a wavelength of 29 nm. A single harmonic order is selected and focused using a pair of normal-incidence multilayer mirrors. The sample stage is positioned near the focus, where it scatters the soft-x-ray beam onto a CCD. Inset: measured logarithmically scaled soft-x-ray beam profile that is a near-Gaussian TEM_{00} over 4 orders of magnitude.

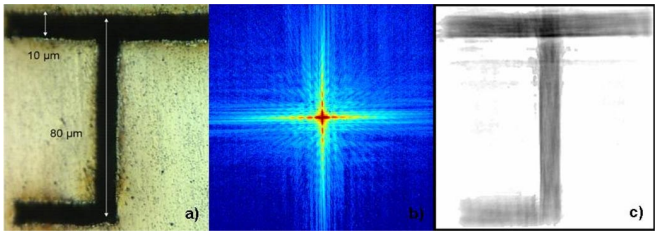

FIG. 2 (color online). (a) Optical image of $\mathcal{J}$ slit. (b) Oversampled diffraction pattern from this sample where the diffraction at the edge of the image corresponds to a momentum transfer of 0.018 nm^{-1}. (c) Magnitude of the reconstructed lensless image.

sampling ratio relates the smallest diffraction pattern speckles to CCD pixels, and it is given by $O = \frac{z\lambda}{pD}$, where p is the pixel size of the CCD camera. For the two images described here, the linear oversampling ratios were $\sim$10. In the reconstructed image, each *image* pixel (not to be confused with a CCD pixel) corresponds to a size d given by $d = \frac{z\lambda}{pN}$, where N is the number of pixels. This image pixel size is thus the ultimate resolution for any given geometry. Another limit on the resolution, r, of the reconstruction is the spectral bandwidth, $\lambda/\Delta\lambda$ of the source, where $r \geq \frac{OD}{\lambda/\Delta\lambda}$ [21]. By inspecting the speckle pattern at high scattering angles, we estimate a spectral bandwidth $>$200.

We used two objects for these experiments: a rectangular $\mathcal{J}$ aperture with a length of 80 μm and a 40 nm thick carbon foil with holes of various sizes (''Quantifoil Multi-A''), placed over a 15 μm diameter aperture. For the $\mathcal{J}$ object, the linear oversampling ratio was 9, with a sample to CCD distance $z = 33$ cm and a sample size $D = 80$ μm, resulting in an image resolution of $\sim$1 μm. For the carbon film, the linear oversampling ratio was 13, with $z = 9$ cm and $D = 15$ μm. Figure 2(b) shows the coherent diffraction pattern from the $\mathcal{J}$ slit. Three different diffraction patterns were stitched together to increase the dynamic range, using a 1 min exposure with no beam block, a 10 min exposure with a $\sim$200 μm beam block, and a 120 min exposure with a $\sim$3 mm beam block.

To reduce noise in the intensity of the final diffraction patterns, we applied an inverse Fourier transform to the measured intensity to obtain the autocorrelation function of the sample. Since the linear oversampling ratio is $\gg 2$, the autocorrelation function is surrounded by a large region that should have no signal. However, because of camera noise that signal is not exactly zero. We therefore applied a low-pass filter to force this region to be zero. We then numerically integrated the diffraction intensity by binning 3×3 pixels into 1 pixel and applying a deconvolution to remove the artifacts in the diffraction pattern due to intensity integration [22]. This step significantly enhanced the signal-to-noise ratio of the coherent diffraction pattern. The analyzed diffraction pattern has a linear oversampling ratio $\sim 1/3$ smaller, and an array size of 680×680 pixels. This also eases the requirement on the temporal coherence by a factor of 3.

Phase retrieval of the coherent diffraction pattern is carried out using the guided hybrid-input-output (GHIO) algorithm [22]. This algorithm starts with 16 independent reconstructions of the diffraction pattern, where random initial phases are used as the input. Each reconstruction iterates back and forth between real and reciprocal space. In real space, a support is defined as a rectangular area containing the sample, with its size estimated from the linear oversampling ratio. The sample density outside the support and the negative real or imaginary part of the electron density inside the support are slowly pushed to zero. In reciprocal space, the magnitude of the Fourier transform (i.e., square root of the diffraction intensity) remains unchanged, and the phase is updated with each iteration. After 2000 iterations, 16 images are reconstructed, which is defined as the 0th generation. An R value is calculated for each image based on the difference between the measured and calculated magnitude of Fourier transform. The image with the smallest R value is selected as the seed. The inputs for the 1st generation are obtained by multiplying the seed with each of the 16 images and taking the square root of the product. We repeat the procedure for the next generation, and after the 8th generation, the 16 reconstructed images became consistent. From the reconstructed images, we define a tight support that represents the true envelope of the object. Using this tight support, we use another GHIO run to obtain the final reconstructed image. Because the diffraction pattern is noncentrosymmetric, the electron density of the sample is complex, which in principle makes the phase retrieval more difficult than for real objects. By using a tight support with GHIO and imposing a positivity constraint on both the real and imaginary parts, we have shown that complex objects can be reliably reconstructed from oversampled diffraction patterns.

Figure 2(c) shows the final image of the $\mathcal{J}$ pattern, with each pixel corresponding to 347 nm. The reconstructed image is consistent with the optical microscope image shown in Fig. 2(a). However, electron density noise can be seen in this image, arising from long-term instability of the EUV source and the finite spectral bandwidth of $\lambda/\Delta\lambda \sim 200$ at 29 nm. When using narrow spectral bandwidth x rays ($\lambda/\Delta\lambda \sim 7500$) from synchrotron radiation sources, this effect is not observed. A lensless image of the carbon film, apertured to 15 μm, is shown in Fig. 3. Figure 3(a) is an SEM picture of the sample, while 3(b) shows the diffraction pattern. The noncentral symmetry of the diffraction pattern indicates that the sample has absorption and that the sample density is complex. Figure 3(c) shows the magnitude of the density for the lensless image, which agrees well with the SEM image. The slight disagreement between the alignment of the holes in the SEM and lensless images is due to parallax. The carbon film and mounting aperture are separated by approximately 56 μm—thus even a few degrees of tilt in the SEM stage slightly alters the parallax and the exact alignment of the smaller holes in the SEM image with respect to the large

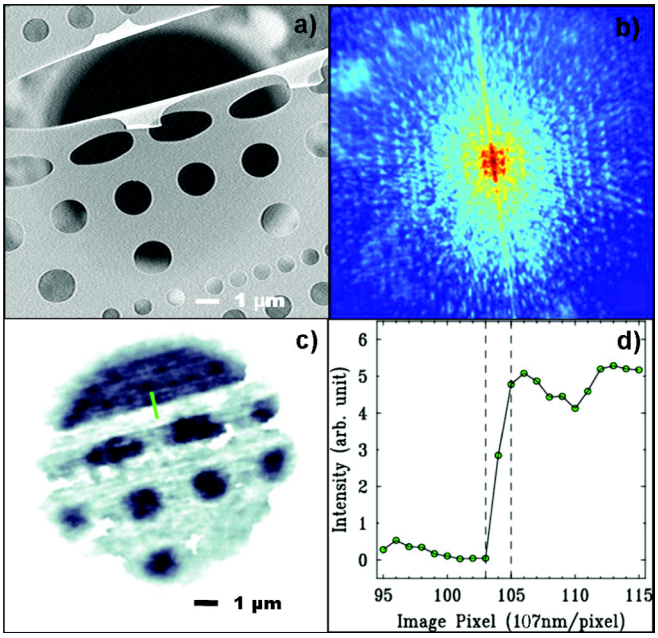

FIG. 3 (color online). (a) SEM image of a masked carbon film; (b) oversampled soft-x-ray diffraction pattern where the diffraction at the edge of the image corresponds to a momentum transfer of 0.059 nm^{-1}; (c) magnitude of the reconstructed lensless image. The correspondence in size, number and position of holes, and aspect ratios between the EUV image and the SEM image can be seen. One pixel in the reconstructed image corresponds to 107 nm. The inset in (c) shows a line scan taken along the direction noted with the green solid line, demonstrating a spatial resolution of 214 nm.

aperture. A line scan of the reconstructed image indicates that the current tabletop lensless microscope has a resolution of 214 nm.

Several aspects of lensless imaging make it an extremely elegant and appealing technique. Because lensless imaging only requires illumination with a plane wave, ~mm accuracy in sample placement is sufficient. No multistep focusing process is necessary, as is the case for imaging systems that require sample placement and stability at the micron level. With imaging optics, the magnification is a purely geometric function of the object to image distance ratio, often requiring the detector to be a meter or more from the imaging optic. In contrast, for tabletop lensless imaging, the entire imaging apparatus fits in 0.5 m × 1.5 m. It should also be noted that the same experimental setup will work at any wavelength at which narrowband coherent light can be produced.

Three approaches are possible for improving the resolution of the microscope. First, higher spatial frequencies could be captured by using a larger detector or a CCD with smaller pixel size. Second, the effective spectral bandwidth of the source could be improved using either narrower band mirrors or by narrowing the individual harmonic peaks. Third, shorter wavelength HHG light could be used. Techniques for selective enhancement of a single harmonic order that can result in narrower bandwidths at shorter wavelengths have recently been demonstrated [23–25]. Such improvements will extend the ultimate resolution to tens of nm. As the laser repetition rates are increased from 3 kHz to tens of kHz, the soft-x-ray flux will be simultaneously increased, and acquisition time will be dramatically reduced from hours to minutes. Also, as computing power increases and reconstruction times shrink, a tabletop soft-x-ray lensless microscope will become increasingly practical for routine use in biological imaging, nanoscience, and metrology in support of next-generation lithography. Moreover, the femtosecond time resolution afforded by high harmonics will enable tabletop time-resolved imaging on femtosecond time scales.

The authors gratefully acknowledge funding from the NSF ERC for EUV Science and Technology and DOE NNSA, and help from the JILA Instrument Shop and the Lehnert labs. R. S. acknowledges financial support from the NSF IGERT program. J. M. acknowledges funding from NSF and DOE. S. Hädrich acknowledges support of DAAD.

*Phone: (303) 210-0396
FAX: (303) 492-5235
Richard.Sandberg@colorado.edu

[1] S. M. Hurtley and L. Helmuth, Science **300**, 75 (2003).
[2] J. C. H. Spence, *Experimental High-Resolution Electron Microscopy* (Oxford University Press, New York, 2003), 3rd ed.
[3] D. Attwood, *Soft X-Rays and Extreme Ultraviolet Radiation: Principles and Applications* (Cambridge University Press, Cambridge, England, 1999).
[4] C. A. Larabell and M. A. Le Gros, Mol. Biol. Cell **15**, 957 (2004).
[5] P. Fischer *et al.*, Mater. Today **9**, 26 (2006).
[6] S. Eisebitt *et al.*, Nature (London) **432**, 885 (2004).
[7] W. Chao, Nature (London) **435**, 1210 (2005).
[8] M. Weiland *et al.*, Ultramicroscopy **102**, 93 (2005).
[9] J. Miao *et al.*, Nature (London) **400**, 342 (1999).
[10] D. Shapiro *et al.*, Proc. Natl. Acad. Sci. U.S.A. **102**, 15 343 (2005).
[11] M. A. Pfeifer *et al.*, Nature (London) **442**, 63 (2006).
[12] H. M. Quiney *et al.*, Nature Phys. **2**, 101 (2006).
[13] J. E. Trebes *et al.*, Science **238**, 517 (1987).
[14] J. Miao *et al.*, J. Opt. Soc. Am. A **15**, 1662 (1998).
[15] J. R. Fienup, Appl. Opt. **21**, 2758 (1982).
[16] H. N. Chapman *et al.*, Nature Phys. **2**, 839 (2006).
[17] R. A. Bartels *et al.*, Science **297**, 376 (2002).
[18] X. Zhang *et al.*, Opt. Lett. **29**, 1357 (2004).
[19] A. Rundquist *et al.*, Science **280**, 1412 (1998).
[20] H. C. Kapteyn, M. M. Murnane, and I. P. Christov, Phys. Today **58**, No. 03, 39 (2005).
[21] J. Miao *et al.*, Phys. Rev. B **67**, 174104 (2003).
[22] C. Song *et al.*, Phys. Rev. B **75**, 012102 (2007).
[23] A. Paul *et al.*, Nature (London) **421**, 51 (2003).
[24] X. Zhang *et al.*, Nature Phys. **3**, 270 (2007).
[25] A. Lytle *et al.*, Phys. Rev. Lett. **98**, 123904 (2007).